General Disclaimer

One or more of the Following Statements may affect this Document

- This document has been reproduced from the best copy furnished by the organizational source. It is being released in the interest of making available as much information as possible.

- This document may contain data, which exceeds the sheet parameters. It was furnished in this condition by the organizational source and is the best copy available.

- This document may contain tone-on-tone or color graphs, charts and/or pictures, which have been reproduced in black and white.

- This document is paginated as submitted by the original source.

- Portions of this document are not fully legible due to the historical nature of some of the material. However, it is the best reproduction available from the original submission.

NASA

Technical Memorandum - 84999

ATMOSPHERIC EFFECTS ON RADIOMETRY FROM ZENITH OF A PLANE WITH DARK VERTICAL PROTRUSIONS

J. Otterman

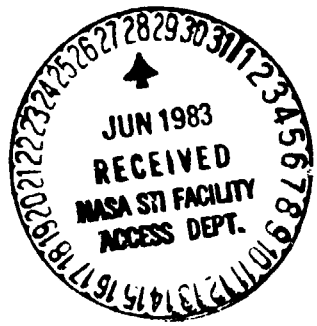

March 1983

National Aeronautics and
Space Administration

Goddard Space Flight Center
Greenbelt, Maryland 20771

However, sandy deserts or sandy playas, with virtually no vegetation, might be an almost unique terrain type in this respect, that they reasonably approximate a Lambert surface when observed from the zenith. Vegetated areas or urban areas can hardly be regarded as planar, because most plants and buildings form sharp protrusions from the plane of the soil. Whether the protrusions are on a scale of a blade of grass or of a skyscraper is immaterial; in either case, the protrusions invalidate the Lambert Law for the surface reflectivity[4,5]. Thus, the analysis of 9 Landsat passes, all within one year, over a presumably unchanging surface (an ungrazed rangeland in Utah), showed variations in the reflectivity by about 25% in all the spectral bands, from the January and December lows to the June highs. The variations were largest in the 0.8–1.1 μm band (~30%) and smallest in the 0.5–0.6 μm band. The effect can be explained as a systematic dependence on the solar zenith angle of the reflectivity to the zenith of the surface. The plants in this arid steppe form 10 to 20 cm high tussocks or bushes protruding from the soil[5]. Their shadows, which depend on the solar elevation, quite obviously reduce the observed reflectivity in winter as compared to summer, for observations at a fixed local time. (Landsat is in a sun-synchronous orbit, with the subsatellite local time at about 09:30 h). The infrared to red reflectivities ratio of this site remains essentially constant throughout the year. The measured reflectivities of a playa, a few kilometers away, also remain approximately constant.

The author's own interest in the problem started with the observations of a fenced-off area in the Sinai, where a rapid recovery of the natural vegetation took place after the entry of the grazing herds was stopped by the fence[3]. The plants consist of mostly grey or dark brown twigs. The green components are quite inconspicuous, except in the desert-bloom period following a rain. Each plant forms an isolated clump, with large interstices of bare soil between a plant and its neighbors, see Fig. 1, in order to draw moisture from a large area. In this study, we analyze the atmospheric effects that can complicate the task of monitoring such a desert-fringe area from a nadir-viewing satellite.

Monitoring a non-Lambertian surface by radiometric imaging from a satellite can be rather difficult, inasmuch as there is no simple correspondence between the differences in the value of the reflectivity measured at different satellite passes, and the possible changes in the surface.

than those over a Lambert plane for the same surroundings-to-object-pixel contrast and atmospheric conditions. However, the adjacency effects are highly variable, because the effective contrast for our plane with dark protrusions is a function of not only the surface parameters but also of the solar zenith angle and the atmospheric conditions.

ATMOSPHERIC EFFECTS ON RADIOMETRY FROM ZENITH OF A PLANE WITH DARK VERTICAL PROTRUSIONS

1. Introduction

In previous studies atmospheric effects on radiometric imaging from Landsat were analyzed. The effects are found to be quite small when three conditions are met: (i) the surface is bright, surface reflectivity larger than 0.20, (ii) the imaged area consists of large homogeneous fields, and (iii) the atmospheric absorption is small. This conclusion can be reached through radiative transfer calculations assuming an appreciable scattering optical thickness, as analyzed by Otterman and Fraser[1]. Alternatively, the effects can be assessed resorting to a simplified radiative transfer treatment for an optically thin atmosphere, as formulated by Otterman et al[2]. Lambert law was assumed for the surface reflection in both papers. This assumption is quite generally made in such studies.

Another approach to this problem area is experimental in nature: a direct comparison of the satellite-measured surface-atmosphere system reflectivities with those of the surface obtained from field measurements. The comparisons involving different parts of the sandy Sinai Desert showed a close correspondence between the surface spectral reflectivities, determined from the Landsat Multispectral Scanner System (MSS) digital data, with only a very small atmospheric correction, and those determined in the field using a hand-held Exotech -100 radiometer[1,3]. The exception was the 0.7-1.1 μm MSS band, where a significant correction for water vapor absorption appeared appropriate.

The Landsat measurements support the assumption of the Lambert law for the surface reflection, inasmuch as the surface reflectivities of these sandy areas, bare of vegetation (northern Sinai and also Mexico near the Colorado River) derived at various times of the year (various solar zenith angles) are essentially constant: the variations in the reflectivity measured on different dates are small, and no systematic dependence in these variations with the solar zenith angle was reported[1].

However, sandy deserts or sandy playas, with virtually no vegetation, might be an almost unique terrain type in this respect, that they reasonably approximate a Lambert surface when observed from the zenith. Vegetated areas or urban areas can hardly be regarded as planar, because most plants and buildings form sharp protrusions from the plane of the soil. Whether the protrusions are on a scale of a blade of grass or of a skyscraper is immaterial; in either case, the protrusions invalidate the Lambert Law for the surface reflectivity[4,5]. Thus, the analysis of 9 Landsat passes, all within one year, over a presumably unchanging surface (an ungrazed rangeland in Utah), showed variations in the reflectivity by about 25% in all the spectral bands, from the January and December lows to the June highs. The variations were largest in the 0.8–1.1 μm band (~30%) and smallest in the 0.5–0.6 μm band. The effect can be explained as a systematic dependence on the solar zenith angle of the reflectivity to the zenith of the surface. The plants in this arid steppe form 10 to 20 cm high tussocks or bushes protruding from the soil[5]. Their shadows, which depend on the solar elevation, quite obviously reduce the observed reflectivity in winter as compared to summer, for observations at a fixed local time. (Landsat is in a sun-synchronous orbit, with the subsatellite local time at about 09:30 h). The infrared to red reflectivities ratio of this site remains essentially constant throughout the year. The measured reflectivities of a playa, a few kilometers away, also remain approximately constant.

The author's own interest in the problem started with the observations of a fenced-off area in the Sinai, where a rapid recovery of the natural vegetation took place after the entry of the grazing herds was stopped by the fence[3]. The plants consist of mostly grey or dark brown twigs. The green components are quite inconspicuous, except in the desert-bloom period following a rain. Each plant forms an isolated clump, with large interstices of bare soil between a plant and its neighbors, see Fig. 1, in order to draw moisture from a large area. In this study, we analyze the atmospheric effects that can complicate the task of monitoring such a desert-fringe area from a nadir-viewing satellite.

Monitoring a non-Lambertian surface by radiometric imaging from a satellite can be rather difficult, inasmuch as there is no simple correspondence between the differences in the value of the reflectivity measured at different satellite passes, and the possible changes in the surface.

The task of monitoring a complex surface such as shown in Fig. 1 necessitates a quantative assessment of the structure of the clumps/plants that protrudes above the soil-plane, as well as a measurement of the soil-plane reflectivity.

Our analysis here of this difficult radiometry is limited to conditions of a low optical thickness and of a laterally homogeneous atmosphere. Favorable conditions for remote sensing in arid regions exist about 250 days a year. When the conditions are unfavorable, the aerosol optical thickness can be quite high. This, by itself, does not necessarily preclude classification of large fields by remote sensing from satellites[6]. However, associated with a large optical thickness, pronounced inhomogeneities are often encountered in the horizontal distribution of the aerosols. Such inhomogeneities can increase the difficulty in the quantitative remote sensing of the surface from satellites.

We present first the previously developed surface model[5,7] aimed at describing the reflectivities of the terrain type shown in Figure 1. A treatment of the atmospheric effects over such a plane with sparse protrusions is then developed. Subsequently, these effects are analyzed in a comparison with those over a Lambert plane.

2. The Surface Reflectivities of a Plane with Sparse Protrusions

The plants are modeled as thin vertical cylinders rising from the horizontal plane of the soil. The model is specified by only one geometrical parameter, s, which is the product of the height, diameter and number of cylinders per unit area (s is dimensionless). The soil and the cylinder mantles (the vertical area of the protrusions) are assumed as of a definite Lambertian reflectivity, r_i for the soil interstices and r_c for the cylinders. The shadow cast on the horizontal plane of the soil by a single cylinder or several cylinders with a projection s on a vertical plane, is $s \tan \theta_0$. It means that a fraction of $1-s \tan \theta_0$ of a parallel beam at a zenith angle θ_0 is intercepted by the soil and a fraction $s \tan \theta_0$ by the cylinders. This holds true as long as the shadow of one cylinder does not fall in part on another cylinder. With lengthening shadows, this assumption and the model become inaccurate. Eventually, at large solar zenith angles, the model breaks down.

Overlapping of shadows can be taken into account if these fractional direct fluxes are expressed by exponentials in $-s \tan \theta_o$, rather than by the linear terms. The fractional direct flux is then $\exp(-s \tan \theta_o)$ on the soil and $1 - \exp(-s \tan \theta_o)$ on the cylinders. These expressions can be derived assuming a random distribution of cylinder-to-neighbor distances and azimuths. This assumption should not be regarded as rigorously correct for any ecosystem, and especially not under the conditions of extreme aridity, where the requirement for a certain minimal plant-to-neighbor distance produces a fairly regular spacing of the protrusions. We stress thus the approximate nature of our model. In this study, we make one more approximating assumption, that the protrusions are non-reflecting, that is, $r_c = 0$.

The surface reflectivity to the zenith accrues only from the interstices, inasmuch as the thin protrusions cannot be observed viewing to the nadir. In this direction the bidirectional reflectivity r_p for the direct solar beam or any beam at zenith angle θ_o, is the product of the soil reflectivity r_i and the fractional flux on the soil plane:

$$r_p\ (\eta_o,\ s,\ r_i) \ = \ r_i \exp(-s\eta_o) \qquad (1)$$

where $\eta_o = \tan \theta_o$.

Throughout the paper, the bidirectional reflectivity is formulated as π times the radiance, resulting from an irradiance of 1 on a horizontal plane. In the case of a Lambert plane, the bidirectional reflectivity of the surface thus defined equals the hemispheric reflectivity (spectral albedo). There is no implication, certainly, that this holds for our surface. Thus, r_p does not equal the hemispheric reflectivity, unless $s = 0$. The hemispheric reflectivity for a plane with sparse protrusions was derived and discussed elsewhere[7].

In field measurements of reflectivity, the reflectivity for the global irradiance is measured. The reflectivity r_p for the direct beam equals the field measurements only when these are conducted at a specific solar elevation, as discussed later.

3. The Reflectivity to the Zenith of the Surface-Atmosphere System for a Plane with Sparse Protrusions.

3.1 Approach to the Calculation

A plane parallel scattering atmosphere is assumed of a low vertical optical thickness τ, $\tau << 1$. The distribution with height of the scatterers is arbitrary. The simplified single scattering approximation (SSS) is used, as introduced into the same problem by Otterman and Fraser[8]: the number of the scattered photons is exactly represented, but the second and higher order scattering events are disregarded. In other words, the direction of a photon after the first scattering is frozen, and cannot be changed by subsequent encounters. This assumption applies to the photons scattered from the direct solar beam, as well as to those scattered from the flux reflected from the soil plane.

A point-symmetrical phase function is assumed for the scatterers, that is, we assume an equal probability of scattering into each of any two opposite directions. The expressions obtained in the analysis apply thus directly to the Rayleigh as well as to the isotropic scattering. The downward directed pencils of the scattered radiation are represented by an equivalent flux. The magnitude of the flux at the surface (above the protrusions) is represented as half of the total scattered from the beam, that is, as $0.5\ [1 - \exp(-\tau/\mu_0)]$, where $\mu_0 = \cos\theta_0$. The accuracy of this representation, analyzed elsewhere[9], is satisfactory for our purposes. The average zenith angle of the flux scattered downward from the direct solar beam, calculated so that the illumination of *the soil-plane* is the same as by the scattered pencils, is separately analyzed[10].

We compute the radiance to the satellite at the zenith from an area within the field of view of its radiometer. We refer to this area as the object pixel. We initially assume that the surface is laterally uniform. In a later part we modify the solution to derive the adjacency effects of cross radiance and of cross irradiance, for a small object pixel embedded in a different, uniform, infinite terrain.

The reflectivity to the zenith r_n of a surface-atmosphere system can be expressed in a way that applies to a Lambert plane as well as to our complex surface, as

$$r_n(\theta_o, \tau, s, r_i) = r_i \frac{G_i^*(\theta_o, \tau, s)[\exp(-\tau) + F^*(\tau, s)]}{1 - 2 r_i B^{**}(\tau, s)} + E(\theta_o, \tau), \qquad (2)$$

where E expresses the backscattering by the atmosphere to the satellite of the solar beam. G_i^* is the fractional irradiance on the soil-plane (the interstices) by the solar beam and by the flux scattered from it. $2B^{**}$ is the fraction of the flux reflected from the soil-plane that is backscattered by the atmosphere to the soil-plane. F^* expresses the scattering to the zenith over the object pixel of the flux reflected from the entire soil-plane, and where $\exp(-\tau)$ represents the extinction of the radiance from the object pixel on the vertical path to the satellite. In this paragraph and throughout the paper, the word soil-plane is not synonymous with the surface: in all the starred parameters, the probabilities of non-interception by the protrusions for the solar beam or for the pencils of the scattered or of the reflected radiation are incorporated. This non-interception has to be assessed on the downleg in G_i^*, on the upleg in F^*, and both on the upleg and the downleg in B^{**}. Obviously, if $s = 0$, all the probabilities of non-interception are 1 and our equation reverts then to one for a Lambert plane with a reflectivity r_i.

3.2 The Atmospheric Backscattering Term, $E(\theta_o, \tau)$, or Airlight

The atmospheric backscattering term E describes the radiance scattered to the satellite from the direct solar beam. This term is completely independent of the surface boundary, and can be referred to as the veil term. The solar irradiance on a horizontal plane at the top of the atmosphere is 1. The total of the fluxes scattered from the direct beam is $1 - \exp(-\tau \mu_o)$ where $\mu_o = \cos \theta_o$. Applying the SSS approach, the radiance to the zenith is expressed as $[1 - \exp(-\tau \mu_o)]\ P(180° - \theta_o)$, where the phase function P is normalized so that its integral over 4π is 1. Multiplying this radiance by π, as is our convention for the bidirectional reflectivity, the atmospheric backscattering or the veil term in Equation (2) is

$$E(\theta_o, \tau) = \pi[1 - \exp(-\tau \mu_o)]\ P(180° - \theta_o). \qquad (3)$$

For the limiting case $(\tau/\mu_0) \to 0$, $E(\theta_0, \tau) \approx \pi \tau P(180° - \theta_0)/\mu_0$. This expression becomes $\tau/4\mu_0$ for the isotropic scattering and $(3\tau/16)[(1/\mu_0) + \mu_0]$ for the Rayleigh scattering.

3.3 The Irradiance $G_i^*(\theta_0, \tau, s)$ on the Soil-Plane.

The irradiance by the direct beam above the surface (above the protrusions) is $\exp(-\tau/\mu_0)$, and the irradiance by the direct beam on the soil-plane is then $\exp(-\tau/\mu_0) \exp(-s\,\eta_0)$. The downward-directed flux scattered from the direct beam is given by the SSS approach in the case of a phase function with point-symmetry as $[1 - \exp(-\tau/\mu_0)]/2$. The fractional error of this representation of the downward flux is $0.15\,\tau^2/\mu_0$.[9] Only a certain fraction of this flux on the surface penetrates through the protrusions to the soil-plane. We denote this fraction $\exp(-s\,\eta_x)$, where $\eta_x = \tan\theta_x$, and θ_x is the effective (average) zenith angle for this penetrating fraction. When the distribution with the zenith angle of the irradiance $L(\vartheta)\cos\theta$ on a horizontal plane scattered from the direct beam is specified, the angle θ_x can be computed by integration:

$$\exp(-s\,\eta_x) \int_0^{\pi/2} L(\theta)\cos\theta\sin\theta d\theta = \int_0^{\pi/2} L(\theta)\cos\theta\sin\theta\exp(-s\tan\theta)\,d\theta\,. \qquad (4)$$

The effective zenith angle θ_x depends thus not only on θ_0 and the phase function of the scatterers, but also on the protrusion parameter s. For a phase function such as that in the Rayleigh scattering, θ_x changes only within narrow limits as a function of θ_0. We assume that θ_x is independent of θ_0. Variable absorption, in a layer close to the surface, such as by water vapor, can produce a marked change in θ_x.[10] In the numerical examples, below, we consider only one value of θ_x, such that $\eta_x = 1.2$, as applicable to a low value of s, in cases of a predominantly isotropic scattering and of significant absorption near the ground. An inappropriate selection of η_x causes only small errors when s is small. The problem vanishes if $s = 0$.

The expression for the fractional solar irradiance on the soil-plane stands now as

$$G_i^* (\theta_o, \tau, s) = \exp(-s\,\eta_o) \exp(-\tau/\mu_o) + 0.5 \exp(-s\,\eta_x) [1 - \exp(-\tau/\mu_o)]$$

$$= \exp(-s\,\eta_o) \left\{ \exp(-\tau/\mu_o) + 0.5 \exp[-s(\eta_x - \eta_o)] [1 - \exp(-\tau/\mu_o)] \right\} \quad . \qquad (5)$$

Equation (5) in its last version is formulated to demonstrate that atmospheric scattering *redirects* a fraction $0.5 [1 - \exp(-\tau/\mu_o)]$ of the solar beam from a direction θ_o to the direction θ_x. In analyzing the atmospheric effects the consequences of this redirection are assessed. This redirrection obviously does not affect the reflectivity in the case of a Lambert plane. The other half of the flux scattered from the direct beam is backscattered out of the surface-atmosphere system, thus reducing the irradiance G_i^*. This reduction does not depend on the surface characteristics.

3.4 The Fraction Backscattered to the Soil-Plane of the Flux Reflected from it, $2B^{**} (\tau, s)$, (Cross Irradiance).

The factor $2B^{**}$ describes the fraction backscattered to the soil-plane of the flux reflected from it. This factor carries a multiplier r_i when contributing to the increase in the global irradiance G_i^* of the soil plane, which is stated as

$$G_t^* (\theta_o, \tau, s) = G_i^* (\theta_o, \tau, s) \left\{ 1 + 2r_i\, B^{**}(\tau, s) + [2r_i\, B^{**} (\tau, s)]^2 \ldots . \right\}$$

$$= \frac{G_i^*(\theta_o, \tau, s)}{1 - 2r_i\, B^{**}(\tau, s)} \quad . \qquad (6)$$

This simple formulation will not generally hold for an arbitrary complex surface: the flux backscattered to the surface will generally be distributed differently with the zenith angle (that is, effectively from a different direction) after each additional backscattering, and thus will have a different probability of penetrating to a specified surface element. Equation (6) applies for our plane with sparse protrusions, because the reflecting element is a horizontal Lambert plane and because the protrusions are assumed in our model to be located at random with respect to the illuminated/shadowed areas. Thus, the effective direction of a reflection does not depend on the

direction of illumination, and will be the same for any illumination of the soil-plane.

The factor $2B^{**}$ represents the probability of the atmospheric backscattering and also the probability of non-interception by the protrusions on the upleg, for the flux reflected from the soil-plane, as well as for the downleg, for the backscattered flux. We introduce a factor B^* such that

$$\exp(-s\,\eta_r)\,B^*(\tau, s) = B^{**}(\tau, s) \tag{7}$$

where $\theta_r = \tan^{-1}\eta_r$ represents the effective zenith angle for the interception by the protrusions of the backscattered flux. We assume later in the numerical examples $\theta_r = \theta_x$.

In formulating the expression for $2B^*$, we consider a pencil of radiation $\cos\theta/\pi$ reflected from the soil-plane at a zenith angle θ. The zenith angle is denoted θ, $0 \leq \theta \leq \pi/2$, on the upleg as well as on the downleg. The solid angle for all such pencils at an angle θ is $2\pi\sin\theta d\theta$. The probability for these pencils to avoid interception by the protrusions and reach the atmosphere is $\exp(-s\tan\theta)$. A nonintercepted pencil has a probability $[1 - \exp(-\tau/\cos\theta)]/2$ of being backscattered to the surface (where the penetration to the soil-plane for the entire backscattered flux is $\exp(-s\,\eta_r)$. Summing the backscattering from all the nonintercepted pencils, $2B^*$ can be stated as

$$2B^*(\tau, s) = \int_0^{\pi/2} \cos\theta\sin\theta\,\exp(-s\tan\theta)\,[1 - \exp(-\tau/\cos\theta)]\,d\theta \tag{8}$$

For the limiting case $(\tau/\cos\theta) \to 0$ and for a Lambert plane ($s = 0$), B^* is the backscattering optical thickness $\tau/2$. As a numerical example consider $\tau = 0.1$, and a bright Lambert surface, $r_i = 0.4$. The term $r_i^2\,2B^{**}$ constitutes then about 4% of the reflectivity r_i. It is even a smaller fraction for a low reflectivity Lambert surface. For a plane with protrusions, the term $r_i\,2B^{**}$ is reduced, due to the factors $\exp(-s\,\eta_r)$, see Equation (7), and $\exp(-s\tan\theta)$ in the integral in Equation (8).

3.5 Factor $F^*(\tau, s)$ for the Radiance Scattered to the Zenith Out of the Flux Reflected from the Soil-Plane (Cross Radiance)

In Equation (2), $r_i\,G_i^*/(1 - 2r_i\,B^{**})$ is the flux reflected from the soil-plane. In this

subsection the radiance scattered to the zenith over the object pixel out of this reflected flux is calculated, summing up the contributions from the reflection over the entire soil-plane. However, we actually calculate the scattering to the zenith over the entire plane from the flux reflected from a unit area. Then we involve the reciprocity law, to obtain the radiance to the zenith over the object pixel accruing by scattering from the pencils of radiation reflected from the entire plane.

Consider a pencil of radiation $r_i \cos\theta/\pi$ reflected from a unit area of the soil-plane at a zenith angle θ. The solid angle for all the pencils at the same zenith angle is $2\pi \sin\theta d\theta$. A fraction $\exp(-s\tan\theta)$ of these reflected pencils will avoid interception by the protrusions. A fraction $1 - \exp(-\tau/\cos\theta)$ of a pencil that penetrates through the protrusions will be scattered by the atmosphere. The radiance to zenith will be a product of the irradiance of $G_i/(1 - 2r_i B^{**})$, of all the terms mentioned above and of $P(\theta)$, the phase function for the angle between a pencil and the zenith. Therefore the parameter F^* which describes this radiance in Equation (2), where it carries a multiplier $r_i G_i/(1 - 2r_i B^{**})$, is

$$F^*(\tau, s) = 2\pi \int_0^{\pi/2} \sin\theta\cos\theta\exp(-s\tan\theta)\, P(\theta)\, [1 - \exp(-\tau/\cos\theta)]\, d\theta, \qquad (9)$$

where we have multiplied by π, as is our convention in expressing the reflectivity r_n in terms of the component radiances, see Equation (2).

The radiance that we discuss in this subsection accrues from the reflection over the entire plane and affects the signal to the satellite over the object pixel. The phenomenon has been termed cross radiance by Otterman and Fraser[8]. It is further discussed in the subsection on the adjacency effects. We note that the protrusions (through the factor $\exp(-s\tan\theta)$ in the integrand) reduce the value of F^* as compared to the cross radiance for the Lambert plane. The reduction is more pronounced for isotropic scattering than for the Rayleigh phase function, which peaks for θ close to zero. In the absence of protrusions, $s = 0$, and in the limiting case $(\tau/\cos\theta) \to 0$, $F^*(\tau, 0) \approx \tau/2$ for any point-symmetrical phase function. $F^*(0.1, s)$ is tabulated

for the isotropic and the Rayleigh phase functions in Table 1, for six values of s ranging up to 0.30. For a limiting thin atmosphere, $F^*(\tau \to 0, s) = \tau f^*(s) = B^*(\tau \to 0, s) = \tau b^*(s)$.

3.6 Assessment of the Atmospheric Effects for a Uniform Plane

We analyze the effects of a scattering atmosphere on the radiometric imaging of the surface, by comparing effects over a plane with sparse, dark protrusions, to those over a Lambert plane. It should be quite clear from our discussion that our results do not constitute a complete solution for complex surfaces where a significant reflection occurs from the vertical walls of the protrusions. Even though such reflected pencils do not directly reach a satellite at the zenith, atmospheric scattering from these pencils of radiation does affect the radiance received at the satellite. We first reformulate Equation (2) for the radiance to the zenith r_n in terms of the reflectivity r_p of our plane with protrusions, rather than in terms of the reflectivity r_i:

$$r_n(\theta_o, \tau, s, r_i) = r_p(\eta_o, s, r_i) \frac{\left\{\exp(-\tau/\mu_o) + 0.5\, \zeta_d(\eta_o, s)\, [1 - \exp(-\tau/\mu_o)]\right\} [\exp(-\tau) + F^*(\tau, s)]}{1 - 2r_p(\eta_o, s, r_i)\, \zeta_r(\eta_o, s)\, B^*(\tau, s)} + E(\theta_o, \tau) \qquad (10)$$

Equation (10) is identical to Equation (2), (in which G_i^* is given by Equation (5) and B^{**} is given by Equation (7), and where we substituted

$$\zeta_d(\eta_o, s) = \exp\,[-s(\eta_x - \eta_o)] \quad , \qquad (11)$$

and

$$\zeta_r(\eta_o, s) = \exp\,[-s(\eta_r - \eta_o)] \quad . \qquad (12)$$

We call ζ_d and ζ_r the redirecting factors. In what follows, we make a simplifying assumption that $\eta_r = \eta_x$, and therefore the two redirecting factors are identical, $\zeta_d = \zeta_r = \zeta$. For sun near the zenith, $\eta_o < \eta_x$, the redirecting factors are smaller than 1, and therefore the redirection causes a reduction in the measured radiance r_n. Conversely, when sun is at a low elevation,

$\eta_o > \eta_x$, the redirecting factors are larger than one, causing an increase in the soil-plane irradiance and therefore in the measured radiance (reflectivity). It follows from this discussion that the reflectivity r_p for the direct beam is the same as for the global irradiance only when $\theta_o = \theta_x$. An alternative treatment of the atmospheric effects, in terms of the reflectivity r_g measured in the field at any solar zenith angle, is given in Appendix A.

The differences $r_n - r_p$ are plotted vs. r_p for $\tau = 0.1$ in Fig. 2 for s = 0.2 and s = 0.0. We refer to the $r_n - r_p$ plots as Cs (complex surface) in the cases s = 0.2 and as La (Lambert plane) in the cases s = 0.0. An alternative abscissa, that of r_i, is also indicated by marking each of the graphs at the points where $r_i = 0.1(0.1)0.9$. In the Figure, three pairs of plots are presented: Fig. 2A for $\eta_o = 1.2$ ($\theta_o = 50.2°$), that is, at the solar elevation at which the redirection factor ζ is 1; Figure 2B for $\eta_o = 0.4$ ($\theta_o = 21.8°$), at which the redirection factor is smaller than 1, $\zeta = 0.85$ if s = 0.2; and Fig. 2C for $\eta_o = 2.0$ ($\theta = 63.4°$), at which the redirection factor is larger than 1, $\zeta = 1.17$ if s = 0.2.

We first examine the plots of $r_n - r_p$ for $\eta_o = 1.2$, $\zeta = 1.0$. For $r_p = 0$, the difference $r_n - r_p$ stems from the atmospheric backscattering only (term E), and is therefore the same in the La and in the Cs graph. With increasing surface reflectivity, the difference $r_n - r_p$ accrues (i) from the term E, (ii) from the extinction, the contribution of which to $r_n - r_p$ can be regarded as linearly proportional to the surface reflectivity, and (iii) from the multiple reflections from the surface, caused by the atmospheric backscattering; see Otterman et al.[2] for a fuller discussion of the Lambert-surface case. We concentrate here on the *differences* between $r_n - r_p$ in the case of our complex surface and in the Lambert case for the same value of r_p. The magnitude of this difference we denote as Δ(Cs, La).

For small values of r_p, the differences between the two graphs increase approximately linearly with r_p, but remain small: $\Delta(Cs, La) < 0.01$ for $r_p \leq 0.4$. With increasing r_p, the Cs graph descends more steeply from its E value (for $r_p = 0$) than the La graph. This is due to the smaller value of $F^*(\tau, s)$ for s of 0.2 than that for a Lambert plane, s = 0. F^* can be

regarded here as a partial compensation for the extinction on the upleg. In this context, the extinction on the path object pixel to satellite is described as $1 - \exp(-\tau) - F^* \approx \tau - F^*$. The differences between Cs and La are here almost negligible if the comparison of the two graphs is made for the same values of r_i. For r_p higher than 0.4, the La graph curves upwards, remaining above the -0.01 ordinate, whereas in the Cs graph the upward curvature is small, the graph dipping to the ordinate of about -0.03 for $r_p = 0.7$ ($r_i = 0.9$). The differences Δ(Cs, La) become larger than 0.02 in this region of r_p. The large differences primarily stem from the fact that in the case of Cs plot, the $2\zeta B^*$ factor is very small, and therefore the upward curving of the plot is reduced as compared to the La plot.

Case A, $\theta_o = 50.2°$, has been selected as the first numerical example because the redirection factor is 1. The reflectivity for the scattered irradiance then equals that for the direct beam, and therefore field measurements of reflectivity for the global irradiance determine r_p. Only in those conditions, the difference $r_n - r_p$ represents the difference between the satellite measurements and the field measurements. Case B, $\theta_o = 21.8°$, has been selected because $\eta_o = \tan\theta_o = 0.4$ is much smaller than in case A, and the redirection factor is significantly smaller than 1, $\zeta = 0.85$. We note first in the Figure 2B that the value of E (that is, $r_n - r_p$ for $r_p = 0$) is only slightly reduced as compared to A. While airmass for scattering from the direct beam is smaller by a factor of 0.69, the value of the Rayleigh phase function is significantly larger at the scattering angle of 158° as compared to that at 130°. (In the case of isotropic scattering, the value of $r_n - r_p$ at $r_p = 0$ would have been considerably smaller.) With increasing r_p, the difference Δ(Cs, La) increases approximately linearly with r_p, somewhat faster than in the case A. This faster increase is due to the smaller value of the redirecting factor, in reducing the enumerator of the expression for the Cs curve. The difference between the curves Cs and La is not very large for small values of r_p: Δ(Cs, La) ≤ 0.015 for $r_p \leq 0.4$. For $r_p > 0.4$ the gap between the two graphs opens quite wide. This is, as in case A, due to the upwards curving of the graph La and only insignificant curving of the graph Cs. In case B, the still weaker curving of the graph Cs is caused by the lower value of the redirecting factor

in the denominator of the expression for r_n.

In case C, $\theta_o = 63.4°$, $\eta_o = 2.0$, the two graphs virtually coincide, that is, Δ(Cs, La) is practically insignificant. The similiarity of the atmospheric effects applies only if a comparison is for the same value of r_p. This is due to the large value of the redirecting factor, $\zeta = 1.17$. However, in the Cs graph, the values of r_p are much smaller than the corresponding r_i. Obviously, there are large differences between the two graphs if a comparison is made for the same value of r_i.

4.0 Adjacency Effects for a Small Pixel Surrounded by a Uniform Terrain

In this section the atmospheric adjacency effects are analyzed for a specific situation, when a small area (the object pixel) is surrounded by a different terrain extending as a uniform area to infinity. Both the object pixel and the surrounding terrain are represented as a plane with sparse protrusions. By introducing s = 0, either one can become a Lambert surface. We recapitulate now our formulation of the surface-atmosphere system reflectivity, as consisting of four terms: veil, signal, cross irradiance and cross radiance.

The veil term $E(\theta_o, \tau)$, see Equation (3), is entirely independent of the surface characteristics. Thus, it can be defined as the reflectivity of the surface-atmosphere system if the surface is black (non-reflecting). The signal term constitutes the additional reading (that is, in addition to E) registering at the radiometer if the object pixel does reflect (surface parameters r_i, s), whereas the surrounding terrain is black. It is given as

$$SR = r_p(\eta_o, s, r_i)\left\{\exp(-\tau/\mu_o) + 0.5\, \zeta_d\, (\eta_o, s)\, [1 - \exp(-\tau/\mu_o)]\right\} \exp(-\tau) \quad . \quad (13)$$

where r_p is given by Equation (1). In this expression for the signal term it is assumed that the dimensions of the object pixel are vanishingly small as compared to the effective height of the scattering layer; the cross radiance and cross irradiance among the elements *within* the object pixel are negiected.

The cross radiance term is the additional reading at the satellite (in addition to E) if the object pixel is black, whereas the entire surrounding plane does reflect, characterized by $\bar{r}_i$ and $\bar{s}$. The cross radiance term is given as

$$\overline{CR} = \frac{\bar{r}_p(\eta_o, \bar{s}, \bar{r}_i)\left\{\exp(-\tau/\mu_o) + 0.5\bar{\zeta}_d(\eta_o, \bar{s})\,[1 - \exp(-\tau/\mu_o)]\right\}\bar{F}^*(\tau, s)}{1 - \bar{r}_p(\eta_o, \bar{s}, \bar{r}_i)\,\bar{\zeta}_r(\eta_o, \bar{s})\,\bar{B}^*(\tau, \bar{s})}, \quad (14)$$

where the barred parameters refer to the entire plane, which is assumed uniform, except for the small object pixel. This explicitly presented term with F* is identical to the cross radiance CR as implicitly given (without the bars) in Equation (10) for $\bar{s} = s$ and $\bar{r}_i = r$.

The cross irradiance term results from a reflection by the surface within the object pixel of the additional irradiance, by the atmospheric backscattering of the flux reflected from the entire plane. The cross irradiance term is

$$\overline{CI} = r_p(\eta_o, s, r_i)\,\zeta_r(\eta_o, s)\frac{\left\{\exp(-\tau/\mu_o) + 0.5\bar{\zeta}_d(\eta_o,\bar{s})[1 - \exp(-\tau/\mu_o)]\right\}\bar{r}_p(\eta_o,\bar{s},\bar{r}_i)\bar{\zeta}_r(\eta_o,\bar{s})\bar{B}^*(\tau,\bar{s})\exp(-\tau)}{1 - \bar{r}_p(\eta_o, \bar{s}, \bar{r}_i)\bar{\zeta}_r(\eta_o, \bar{s})\,\bar{B}^*(\tau, \bar{s})} \quad (15)$$

This complicated expression for the cross radiance is also implicitly included in Equation (10), where $\bar{s} = s$ and $\bar{r}_i = r_i$.

In what follows, the term $r_p\zeta_r B^*$ in the denominator of both $\overline{CR}$ and CR is neglected. This reduces the values of $\overline{CR}$ and CR by only about 1%. (The fractional error in the difference $\overline{CR}$ - CR can be larger, however). The simplified expressions for $\overline{CR}$ and CR are denoted as $\widetilde{\overline{CR}}$ and $\widetilde{CR}$. Our concern is an assessment of the fractional uncertainty or error in measuring the surface reflectivity, introduced by the adjacency effects. We refer to the expression for this uncertainty as the fractional difference in cross radiance, $\Delta\widetilde{FCR}$. It is obtained dividing $\overline{CR}$ - CR by the signal component SR, (see Equation 13):

$$\Delta\widetilde{FCR}\,(\theta_o, \tau, \bar{s}, s, \bar{r}_i, r_i)$$

$$= \left\{\frac{\bar{r}_p(\eta_o, \bar{s}, \bar{r}_i)\left\{\exp(-\tau/\mu_o) + 0.5\bar{\zeta}_d(\mu_o, \bar{s})\,[1 - \exp(-\tau/\mu_o)]\right\}}{r_p(\eta_o, s, r_i)\left\{\exp(-\tau/\mu_o) + 0.5\bar{\zeta}_d(\mu_o, s)\,[1 - \exp(-\tau/\mu_o)]\right\}}\,\bar{F}^*(\tau, \bar{s}) - F^*(\tau, s)\right\}\exp\tau$$

$$= [C(\theta_o, \tau, \bar{s}, s, \bar{r}_i, r_i)\,\bar{F}^*(\tau, \bar{s}) - F^*(\tau, s)]\,\exp\,\tau. \quad (16)$$

where the parameter

$$C(\theta_o, \tau, \bar{s}, s, \bar{r}_i, r_i) = \frac{\bar{r}_p(\eta_o, \bar{s}, \bar{r}_i)\left\{\exp(-\tau/\mu_o) + 0.5\ \bar{\zeta}_d(\eta_o, \bar{s})\ [1 - \exp(-\tau/\mu_o)]\right\}}{r_p(\eta_o, s, r_i)\left\{\exp(-\tau/\mu_o) + 0.5\ \zeta_d(\eta_o, s)\ [1 - \exp(-\tau/\mu_o)]\right\}} \quad (17)$$

is the effective contrast ratio between the surroundings and the object pixel.

The factors controlling the adjacency effects are tabulated for various values of s in Table 1. These are: the cross radiance factors for a finite optical thickness for Rayleigh scattering

$$F_m^*(\tau, s) = \frac{1}{2}\int_0^1 [1 - \exp(-\frac{\tau}{\mu})]\ \exp(-s\ \frac{\sqrt{1-\mu^2}}{\mu})\ (\frac{3}{4} + \frac{3}{4}\mu^2)d\mu \quad (18)$$

where the subscript m stands for molecular scattering, and for isotropic scattering,

$$B^*(\tau, s) = \frac{1}{2}\int_0^1 [1 - \exp(-\frac{\tau}{\mu})]\ \exp(-s\ \frac{\sqrt{1-\mu^2}}{\mu})\ d\mu \quad (19)$$

which is identical to the backscattering factor of the flux reflected from the soil-plane. Those two factors are computed for $\tau = 0.1$. We also present the factors

$$f_m^*(s) = \frac{1}{2}\int_0^1 \exp(-s\ \frac{\sqrt{1-\mu^2}}{\mu})\ (\frac{3}{4} + \frac{3}{4}\mu^2)\ d\mu \quad (20)$$

$$b^*(s) = \frac{1}{2}\int_0^1 \exp(-s\ \frac{\sqrt{1-\mu^2}}{\mu})\ d\mu \quad (21)$$

such that for $\tau \to 0$

$$F_m^*(\tau, s) \to \tau\ f_m(s)$$

and

$$B^*(\tau, s) \to \tau\ b^*(s) \quad .$$

Given the values of the cross radiance factors in Table 1, we can readily assess the adjacency effects in some numerical examples. In the case $\bar{s} = s$, that is, when the protrusion parameter within the object pixel is the same as that of the surrounding terrain, the contrast ratio C is simply $\bar{r}_i/r_i$, a contrast independent of s, θ_o, or τ. The expression for $\Delta\tilde{FCR}$ is

reduced to $(C - 1)\, F^* \exp\tau = (\bar{r}_i - r_i)\, F^* \exp\tau / r_i$ inasmuch as $\bar{F}^* = F^*$. Consider a case $\bar{r}_i = 0.3$ and $r_i = 0.1$, that is, a contrast ratio of 3, and assume Rayleigh scattering and $\tau = 0.1$. For $\bar{s} = s = 0.2$, the adjacency effect $\Delta\widetilde{FCR}$ amounts to 6.8%. Under the same conditions, but for a Lambert surface, $\Delta\widetilde{FCR}$ amounts to 9.5%. We note that the adjacency effect $\Delta\widetilde{FCR}$ is significantly reduced for a plane with sparse protrusions as compared to that for a Lambert surface. The reduction does not depend on the contrast ratio. For the value 0.2 of the protrusion parameter, the reduction is in the ratio $F_m^*(0.1, 0.2)/F_m^*(0.1, 0.0) = 0.031/0.043 = 0.72$ or by 28%.

The general case, when $\bar{s} \neq s$, is more complicated, because the contrast ratio C as defined is a function of $\bar{s}$, s, θ_0 and τ as well as of $\bar{r}_i$ and r_i. Under similar assumptions ($\bar{r}_i = 0.3$, $r_i = 0.1$, Rayleigh scattering and $\tau = 0.1$), consider the case $\bar{s} = 0.2$ and $s = 0.0$. The contrast ratio is 2.65 at θ_0 of 21.8°, 2.36 at 50.2° and 2.05 at 63.4°. The adjacency effect $\Delta\widetilde{FCR}$ at these zenith angles is 4.2%, 3.3%, and 2.2%, respectively. At very large zenith angles $\Delta\widetilde{FCR}$ reverses its sign. The results are quite different when a Lambert surface surrounds a plane with protrusions. If the reflectivities of the soil plane remain respectively $\bar{r}_i = 0.3$ and $r_i = 0.1$, but when $\bar{s} = 0.0$ and $s = 0.2$, the contrast C is 3.41 at zenith angle of 20.3°, 3.81 at 50.2° and 4.39 at 63.4°. The adjacency effect $\Delta\widetilde{FCR}$ increases with the zenith angle, from 12.8% at 20.3°, to 14.7% at 50.2° and to 17.5% at 63.4°.

5.0 Discussion and Conclusions

In this study we addressed the problem of atmospheric interference in radiometric imaging of Earth's land surfaces from satellites. It is our assertion that in most cases land areas should not be represented as a Lambert surface and require a representation as a complex surface. A rather primitive model has been presented here: a Lambertian soil-plane from which dark (absorbing) protrusions arise. The dark protrusions do not contribute to the reflection from the surface. Their effect can be visualized as that of an absorbing layer of thin vertical needles or chaff that float above a horizontal Lambertian plane. Radiative transfer through such a layer

is treated by defining its optical thickness s as a projection on a vertical plane of needles over a unit area. The transmission through the layer as a function of the zenith angle θ is given as $\exp(-s \tan\theta)$. The extinction is zero on a vertical path and tends to infinity on a near-horizontal path. The effects as a function of θ are thus significantly different than those of a plane-parallel layer of gaseous or aerosol absorbers.

The radiative transfer through the scattering atmosphere is treated approximately, applying the simplified single scattering approach. The number of the scattered photons is computed exactly for the direct solar beam and for the radiation pencils reflected from the surface, under the assumption of a plane-parallel atmosphere. The approximation is only that a scattered photon retains the direction after its first scattering even if it undergoes subsequent scatterings.

The effects of the atmosphere are here expressed as the difference between the reflectivity r_n of the surface-atmosphere system measured by a satellite-borne radiometer at the zenith and the reflectivity to the zenith r_p of the complex surface for the direct solar beam. We first report our findings for imaging large, laterally homogeneous areas. The differences $r_n - r_p$ are found quite similar to the differences $r_n - a_o$ when imaging a Lambert surface with a reflectivity a_o, if the comparison is made for $r_p = a_o$. This applies to low and moderate values of r_p, $r_p < 0.4$. For large values of r_p, the difference $r_n - r_p$ becomes more negative than the corresponding $r_n - a_o$. This occurs because for $a_o > 0.4$, the plots $r_n - a_o$ vs a_o curve upwards, due to a term with a_o^2 that describes the second reflection from the surface (of the flux backscattered by the atmosphere). This effect, and thus the upward curvature of the $r_n - r_p$ plots, is sharply reduced in the case of plane with dark protrusions.

We compared the effects over a plane with protrusions, $r_n - r_p$, with those over a Lambert plane, $r_n - a_o$, on the basis of $r_p = a_o$. Because of the protrusions, the reflectivity of the surface is lower than that of the soil-plane (the interstices). The reduction increases with an increasing solar zenith angle. Thus, we can state that the atmospheric effects over plane with protrusions with a reflectivity r_i of the interstices are really comparable with those over a

Lambert surface with a low reflectivity, approximately given as $r_i \exp(-\tan \theta_o)$. For a low reflectivity surface, the backscattering from the atmosphere to the satellite is a more important component of the $r_n - a_o$ difference than for a bright surface. The backscattering to the surface of the flux reflected from it is of little importance. A plane with protrusions can be regarded in this context as a low reflectivity surface, with the reflectivity effectively decreasing with increasing solar zenith angle. Thus, our conclusions apply most forcefully when the sun is low, (see Figure 2C, where r_p for $s = 0.2$ is much lower than r_i).

In imaging areas with dimensions not large compared to the effective height of the scattering layer, adjacency effects have to be considered. We analyze such effects only when the object pixel is a small area different from the surrounding terrain, that stretches to infinity as a uniform surface. This limiting case was analyzed previously for Lambert surface, retaining in the analysis only linear terms in the optical thickness[2]. For a plane with protrusions, the simplest case is when the protrusion parameter s within the object pixel is equal to that in the surrounding terrain, $\bar{s}$. The adjacency effects in this case are significantly lower than in the case of a Lambert surface with the same surroundings-to-object-pixel contrast ratio and the same scattering optical thickness. However, when $\bar{s} \neq s$, the situation is more complex. The magnitude of the adjacency effects can vary pronouncedly with the solar zenith angle, and even the sign can change, because the effective contrast surroundings-to-object-pixel depends on the direction of the illumination of the surface. Limitations of this analysis of the adjacency effects should be noted. When the cross radiance is computed as accruing from fluxes reflected up to a certain distance (rather that over the entire plane), the effect on the radiometry of a small field depends crucially on the shape of the phase function in the forward region.[11]

This study certainly is not the definite treatment of the atmospheric effects on radiometric imaging of land areas. The subject deserves continued studies, applying the approach of modeling and Monte Carlo techniques, in addition to the programs of field measurements of the reflectivity.

Table 1

The parameters F_m^*, B^* (for $\tau = 0.1$), f_m^* and b^*, for various values of s.

s	$F_m^*(0.1, s) \times 10^2$	$B^*(0.1, s) \times 10^2$	$f_m^* \times 10$	$b^* \times 10$
0.30	2.713	2.425	2.946	2.654
0.20	3.078	2.810	3.365	3.103
0.10	3.563	3.339	3.948	3.774
0.05	3.885	3.702	4.359	4.224
0.02	4.121	3.974	4.675	4.602
0.00	4.303	4.188	5.000	5.000

References and Footnotes

1. J. Otterman and R. S. Fraser, Remote Sensing Environ. 5, 441 (1976).
2. J. Otterman, S. Ungar, Y. J. Kaufman and M. Podolak, Remote Sensing Environ. 9, 115 (1980).
3. J. Otterman, Tellus 33, 68 (1981).
4. G. H. Suits, Remote Sensing Environ. 2, 117 (1972); K. T. Kriebel, Appl. Opt. 17, 253, (1978).
5. J. Otterman, Advances Space Res. 1, 115 (1981).
6. R. S. Fraser, O. P. Bahethi and A. H. Al-Abbas, Remote Sensing Environ. 6, 229 (1977).
7. J. Otterman, J. Geoph. Res. 87, 1270 (1982).
8. J. Otterman and R. S. Fraser, Appl. Opt. 18, 2852 (1979).
9. J. Otterman, Explicit Expressions for Fluxes Scattered by an Optically Thin Rayleigh Atmosphere (1983), in preparation.
10. J. Otterman, Y. J. Kaufman, G. Weiss, Effective Zenith Angles of Sky Radiance Scattered to a Complex Surface by an Optically Thin Atmosphere, (1983), in preparation.
11. J. Otterman, M. Dishon and S. Rehavi, Int. J. Remote Sensing 4, in press (1983).

Figure Captions

Figure 1. A 1976 photograph of an exclosure in the northern Sinai, an area fenced off in 1974.

Figure 2. Calculated differences $r_n - r_p$ for a plane with sparse protrusions, s = 0.2 (dashed lines), and for a Lambert surface, s = 0.0 (solid lines), at three zenith angles.

Acknowledgments

This study was completed while the author was a NAS-NRC Senior Research Associate at NASA Goddard Space Flight Center, Greenbelt, MD. Helpful comments by Y. J. Kaufman and R. S. Fraser are gratefully acknowledged.

Figure 1. A 1976 photograph of an exclosure in the northern Sinai, an area fenced off in 1974.

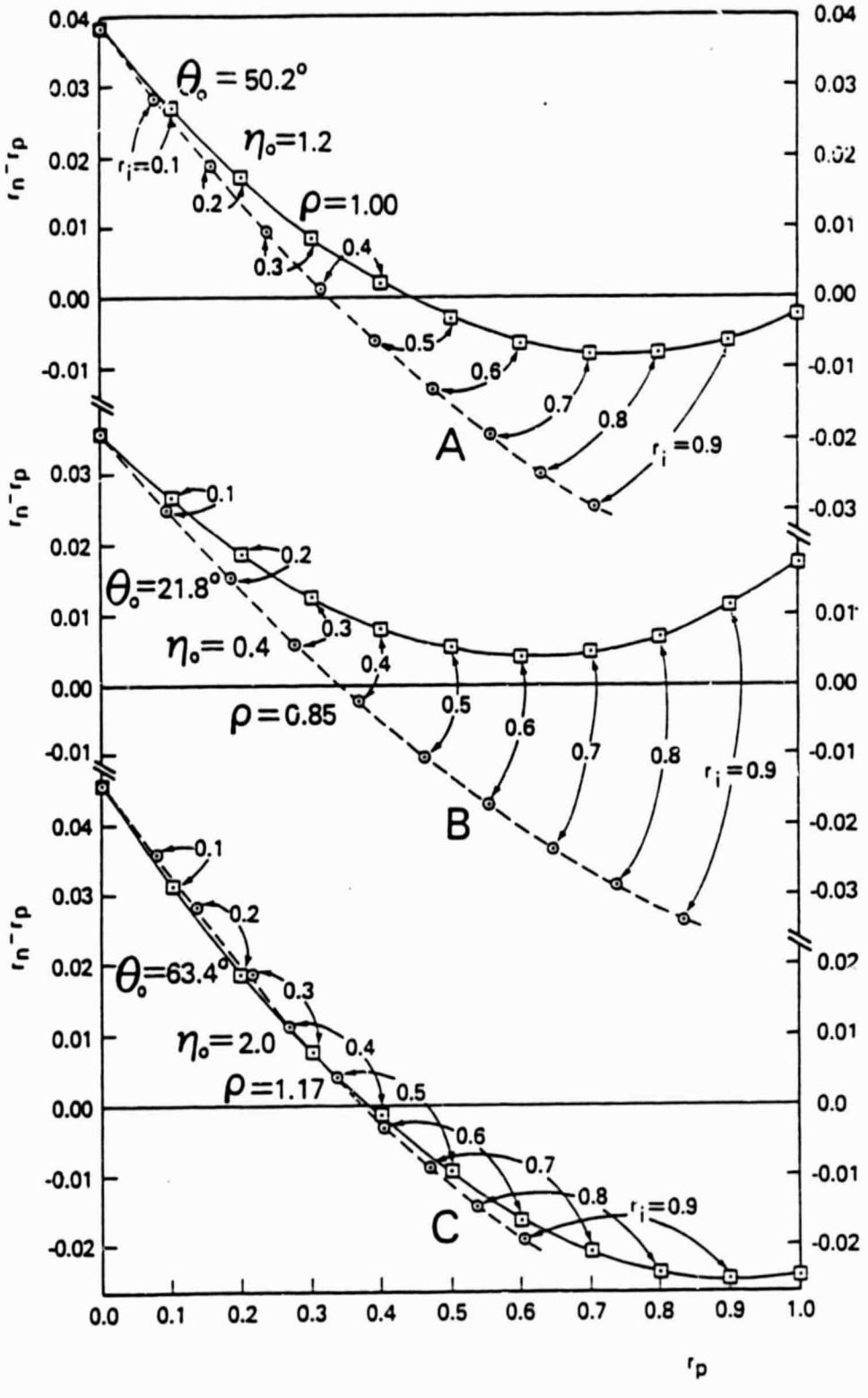

Figure 2. Calculated differences $r_n - r_p$ for a plane with sparse protrusions, s = 0.2 (dashed lines), and for a Lambert surface, s = 0.0 (solid lines), at three zenith angles.

APPENDIX A

The formulation of the atmospheric effects in terms of the reflectivity r_p for the direct beam (that is, as $r_n - r_p$ differences) has the advantage that r_p is given by a simple explicit expression $r_p = r_i \exp(-s \tan\theta_o)$, solely in terms of the surface parameters r_i and s. It is this reflectivity r_p for a direct beam that is measured in the laboratory, whether of an individual plant or an array of plants. The reflectivity measured in the field, which we denote r_g, does *not* equal r_p except when $\theta_o = \theta_x$. (From a practical viewpoint, r_p and r_g, are close enough in value to be considered equal if $45° < \theta_o < 60°$ and the scattering optical thickness is not too large.) Thus, a formulation of the atmospheric effects as the $r_n - r_g$ differences has the distinct advantage of comparing two *measured* quantities, one from the satellite and one from the ground. The significant disadvantage of this approach is that the expression for r_g is more cumbersome than that for r_p, inasmuch as we formulate r_g as accruing from *three* separate streams (rather than a *single* stream in the case of r_p). These streams are: (i) the direct beam, $\mu_o \exp(-\tau/\mu_o)$, that penetrates to the soil-plane at θ_o; (ii) the stream scattered from the direct beam, $0.5\,\mu_o\,[1 - \exp(-\tau/\mu_o)]$, that penetrates effectively at θ_x; and (iii) the stream G_b scattered back to the surface from the flux reflected from it:

$$G_b(\theta_o, \tau, s, r_i) = \mu_o \{\exp(-s\eta_o)\exp(-\tau/\mu_o) + \exp(-s\eta_x)\,0.5\,[1\exp(-\tau/\mu_o)]\} \frac{2r_i\,B^*(\tau,s)}{1 - 2r_i\exp(-s\eta_r)B^*(\tau,s)} \quad \text{(A-1)}$$

that penetrates to the soil-plane at θ_r. The expressions for the magnitudes of the two scattered streams are based on the simplified single scattering (SSS) approach.

As a sum of the responses to these three streams, the surface reflectivity r_g is a function of the atmospheric conditions as well as of the surface parameters and the solar zenith angle:

$$r_g(\theta_o, \tau, s, r_i)$$

$$= r_i \frac{\exp(-s\eta_o)\exp(-\tau/\mu_o) + 0.5\exp(-s\eta_x)[1-0.5\exp(-\tau/\mu_o)] + \exp(-s\eta_r)\, G_b(\theta_o, \tau, s, r_i)}{G_o(\theta_o, \tau, s, r_i)} \quad \text{(A-2)}$$

where the global irradiance G_o on the surface at the top of the protrusions is the sum of the three streams discussed above.

With these explicit relations between r_g and the parameters describing the surface and the atmosphere, and applying the relations presented in the text between r_n and the same parameters, the $r_n - r_g$ differences can be studied.